



NUMERICAL INVESTIGATION OF THE DRAG CRISIS IN FLOW PAST A ROUGH CIRCULAR CYLINDER

Alex Mendonça Bimbato

Luiz Antonio Alcântara Pereira

Institute of Mechanical Engineering, Federal University of Itajubá, Itajubá, CP 50, Minas Gerais, Brazil.

aleximbato@yahoo.com.br

luizantp@unifei.edu.br

Miguel Hiroo Hirata

State University of Rio de Janeiro, FAT-UERJ, Resende, Rio de Janeiro, Brazil

miguelhirata@gmail.com

Abstract. *The present work deals with two-dimensional numerical simulations to study wake structures and flow dynamics past a circular cylinder. Based on a physical sense that roughness surfaces can promote turbulent flows a roughness surface model associated to the second-order velocity structure function model adapted to Lagrangian mesh-free Vortex Method is proposed. A comparison between flow patterns originated from the smooth and rough circular cylinders is presented to demonstrate the ability of the roughness model to represent the physics involved in this kind of problem; the study is focused on the drag crisis. This work shows that the characteristics of high Reynolds number flows are well predicted by a two-dimensional roughness model.*

Keywords: *Roughness Surface Model, Subgrid Model, Aerodynamic of Bluff Body, Flow Patterns, Discrete Vortex Method.*

1. INTRODUCTION

The flow around bluff bodies can cause important physical phenomena, such as separation, vortex shedding and transition to turbulence. The transition to turbulence at a bluff body is one of the most studied phenomena by the scientific community. The parameter that governs the transition to turbulence is the Reynolds number, Re ($Re = U^* d^* / \nu$, where U^* is the incident flow velocity, d^* is the characteristic length and ν is the kinematic viscosity). The transition to turbulence begins at the bluff body wake and, as the Reynolds number increases, it reaches the shear layers, and for higher Reynolds numbers, it reaches the boundary layers.

Nishino (2007) classified the flow around a smooth and isolated circular cylinder in three regimes: subcritical ($Re < 2.0 \times 10^5 - 5.0 \times 10^5$), critical ($Re \cong 2.0 \times 10^5 - 5.0 \times 10^5$) and supercritical ($Re > 2.0 \times 10^5 - 5.0 \times 10^5$); Roshko (1961) included a fourth regime called transcritical ($Re > 3.5 \times 10^6$).

A particular interest surges when the transition to turbulence reaches the boundary layers. When this occurs the flow has more momentum to support the adverse pressure gradient and the separation points move to downstream causing the drag crisis. As the transition to turbulence at the boundary layers occurs at high Reynolds number flows, small perturbations can be amplified and, as consequence, can modify the aerodynamic behaviour of the bluff body. One of the most common perturbations found in engineering applications is the body surface roughness, which can anticipate the transition to turbulence. In order to reduce the flow complexity this paper studies the influence of the circular cylinder roughness surface in a high Reynolds number flow. Although the circular cylinders consist in simple bluff body geometry, many interesting flow characteristics can be studied with this simple shape.

The main difficulty to study turbulent flows around rough surfaces is related to the surface roughness characteristics. The surface roughness can be determined by the following parameters: (i) the relative roughness, ε^*/d^* , where ε^* is the surface protuberance's height and d^* is the circular cylinder diameter; (ii) the surface texture, what indicates how the protuberances are arranged on the surface.

One of the first works that studied the drag coefficient behaviour for a rough circular cylinder was done by Fage and Warsap (1929); they measured the mean drag coefficient, \overline{C}_D , and showed that, as the relative roughness (ε^*/d^*) increased, the drag crisis occurred at lower Reynolds number flows. Zdravkovich (2003) presents more details about the work done by Fage and Warsap (1929).

Güven, *et al.* (1980) showed in a $\overline{C}_D \times Re$ diagram their results with the results obtained by Fage and Warsap (1929), Achenbach (1971) and Szechenyi (1975). The results present differences up to 60% for a given Reynolds number. These differences were attributed to some influencing factors, such as: aspect ratio, blockage ratio, turbulence level and the surface texture. The greater differences were observed in the supercritical flow regime which indicates the

Bimbato, A. M., Alcântara Pereira, L. A. and Hirata, M. H.
Numerical Investigation of the Drag Crisis in Flow Past a Rough Circular Cylinder

importance of the surface roughness. It is known that, in the supercritical flow, the viscous sublayer is too reduced that surface's protuberances cause disturbances in the boundary layer flow.

Buresti (1981) used rough circular cylinders to analyze $\overline{C}_D \times Re$ and $St \times Re$ diagrams (the Strouhal number, St , is a dimensionless parameter used to measure the vortex shedding frequency, f^* (see Eq. (1))). It was observed that the mean drag coefficient decreased and, after reaches a minimum value, it increased slowly. The Strouhal number increased abruptly in the critical flow regime and, after reaches a maximum value, it decreased slowly. The authors attributed the gradual increase of the mean drag coefficient and the gradual decrease of the Strouhal number to a large wake developed downstream the body.

$$St = f^* \frac{d^*}{U^*} \quad (1)$$

Kareem and Cheng (1999) distributed rough cylindrical elements on a circular cylinder surface to study supercritical flow patterns in a subcritical wind tunnel. The Reynolds number was $Re = 25400$. However, the pressure coefficient and the separation point obtained was a typical $Re = 7.0 \times 10^6$ flow. The strategy used by Kareem and Cheng (1999) are usefull, since it is known the difficulty related to the study of high Reynolds number flows in wind tunnels. It can be noted in the literature a lack of numerical simulations at high Reynolds number flows ($Re \geq 1.0 \times 10^5$). An exception is the work done by Kawamura, *et al.* (1986); the authors studied numerically the two-dimensional flow around a rough circular cylinder ($\varepsilon^*/d^* = 0.005$) at $10^3 < Re < 10^5$ using the finite difference method. Kawamura, *et al.* (1986) obtained good results for $\overline{C}_D \times Re$ diagram. However, as they had instability problems with the finite difference method, the obtained $\overline{C}_D \times Re$ diagram did not even reach $Re = 1.0 \times 10^5$. No turbulence model was used by authors.

In the present work a two-dimensional roughness model is developed to be incorporated to a Lagrangian Vortex Method. The roughness model is associated to the second-order velocity structure function of the filtered field (Alcântara Pereira, *et al.*, 2002; Bimbato, *et al.*, 2012). The Lagrangian Vortex Method is used since it has been developed and applied for the analysis of complex, unsteady and vortical flows (Kamemoto, 2004). The most important features of the Discrete Vortex Method (Chorin, 1973; Leonard, 1980; Lewis, 1999; Kamemoto, 2004; Stock, 2007) are: (i) it is a mesh free technique; (ii) it is a suitable technique for large eddy simulation; (iii) the computational efforts are directed only to the regions with non-zero vorticity and not to all fluid domain as is done in the eulerian description; (iv) the far away boundary condition is taken into account automatically.

2. GOVERNING EQUATIONS AND BOUNDARY CONDITIONS

Figure 1 shows the two-dimensional, incompressible and unsteady viscous flow around an isolated circular cylinder, where U^* is the mainstream velocity, Ω is the fluid domain defined by surface $S = S_1 \cup S_2$, being S_1 the body surface and S_2 the far away boundary. The flow depicted in Fig. 1 is governed by the continuity and the Navier-Stokes Equations, which can be written in the form (Alcântara Pereira, *et al.*, 2002):

$$\frac{\partial \bar{u}_i}{\partial x_i} = 0 \quad (2)$$

$$\frac{\partial \bar{u}_i}{\partial t} + \frac{\partial}{\partial x_j} (\bar{u}_i \bar{u}_j) = -\frac{1}{\rho} \frac{\partial \bar{p}}{\partial x_i} + 2 \frac{\partial}{\partial x_j} [(v + v_i) \bar{S}_{ij}] \quad (3)$$

where \bar{u}_i is the velocity filtered field ($u_i = \bar{u}_i + u'_i$; u'_i is the velocity fluctuation), \bar{p} is the pressure filtered field, v_i is the eddy viscosity and \bar{S}_{ij} is the deformation tensor of the filtered field (Smagorinsky, 1963).

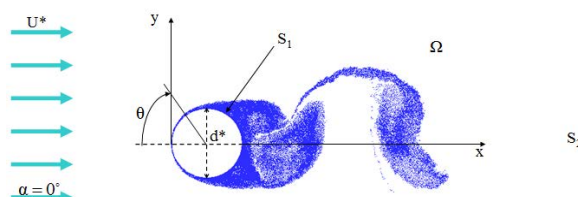


Figure 1. Flow around an isolated circular cylinder

Considering that the small scales are homogeneous and isotropic and using a relation proposed by Batchelor (1953), Lesieur and Métais (1996) proposed to use the local kinetic energy spectrum in order to calculate the eddy viscosity:

$$v_t(\mathbf{x}, \Delta^+, t) = 0.105 C_k^{-3/2} \Delta^+ \sqrt{\overline{F_2}(\mathbf{x}, \Delta^+, t)} \quad (4)$$

where $C_k = 1.4$ is the kolmogorov constant and $\overline{F_2}(\mathbf{x}, \Delta^+, t)$ is the local second-order velocity structure function of the filtered field, defined as:

$$\overline{F_2}(\mathbf{x}, \Delta^+, t) = \left\| \overline{\mathbf{u}(\mathbf{x}, t) - \mathbf{u}(\mathbf{x} + \mathbf{r}, t)} \right\|_{|\mathbf{r}| = \Delta^+}^2 \quad (5)$$

where $\overline{\mathbf{u}(\mathbf{x}, t) - \mathbf{u}(\mathbf{x} + \mathbf{r}, t)}$ is the average speed differences between the center of a sphere located at \mathbf{x} with radius $|\mathbf{r}| = \Delta^+$ and points located on the sphere surface. In this formulation the center of the sphere is defined as a point of the flow field where one wants to calculate the turbulent activity. The above equation is used in three-dimensional flows; since the present work deals with a two-dimensional flow the second-order velocity structure function model needs to be adapted to two-dimensional problems (see Section 3.3).

Therefore Eq. (2) and Eq. (3) are used to simulate the large eddy phenomena with the Discrete Vortex Method and the small eddy ones are taken into account by eddy viscosity (Eq. (4)) which is modeled by local second-order velocity structure function of the filtered field (Eq. (5)).

The impermeability condition, Eq. (6), demands that the normal velocity component of the fluid particle, \overline{u}_n , should be equal to the normal velocity components of the surface S_I , v_n . The no-slip condition, Eq. (7), demands that the tangential velocity component of the fluid particle, \overline{u}_τ , should be equal to the tangential velocity component of the surface S_I , v_τ . The far away boundary condition is given by Eq. (8). The equations are respectively:

$$\overline{u}_n - v_n = 0, \text{ on } S_I \quad (6)$$

$$\overline{u}_\tau - v_\tau = 0, \text{ on } S_I \quad (7)$$

$$|\overline{\mathbf{u}}| \rightarrow U^*, \text{ on } S_2 \quad (8)$$

In order to make all the quantities in the equations above non-dimensional, U^* and d^* are used. The non-dimensional time is given by $t^* U^* / d^*$. In the formulation above the symbol * means dimensional quantities.

3. NUMERICAL SOLUTION: THE LAGRANGIAN VORTEX METHOD

3.1 The Roughness Model

The essence of the Lagrangian Vortex Method is to discretize the vorticity field using Lamb discrete vortices in a manner that (Kundu, 1990):

$$\overline{\boldsymbol{\omega}}(\mathbf{x}, t) = \sum_{k=1}^{NV} \frac{\Gamma_k}{\pi \sigma_{\theta_k}^2} \exp\left(-\frac{|\mathbf{x}|^2}{\sigma_{\theta_k}^2}\right) \quad (9)$$

where $\overline{\boldsymbol{\omega}}$ ($\overline{\boldsymbol{\omega}} = \nabla \times \overline{\mathbf{u}}$) is the vorticity filtered field, NV is the total number of discrete vortices in the fluid domain, Γ_k is the strength of the discrete vortex k necessary to satisfy Eq. (7) and σ_{θ} is the Lamb vortex core given by (Musto, *et al.*, 1998; Bimbatto, 2012):

$$\sigma_{\theta} = 4.48364 \sqrt{\frac{\Delta t}{Re}} \chi \quad (10)$$

The time step Δt is calculated from an estimate of the convective length and velocity scales of the flow. χ is a factor obtained through numerical experiences in order to determine the appropriate value of the Lamb vortex core,

considering the influence of the method used to represent the solid boundaries; more details can be found in Bimbato (2012).

In this work the circular cylinder surface is represented by source flat panels (Katz and Plotkin, 1991). Each panel has a pivotal point where Eqs. (6) and (7) must be imposed. The sources strength distributed along the flat panels satisfy Eq. (6). A Lamb discrete vortex is positioned at a shedding point defined near each flat panel to satisfy Eq. (7). Figure 2(a) shows one of the source flat panels used to represent the circular cylinder surface; it illustrates how the vorticity is generated on a smooth surface by the Vortex Method (co_i is the pivotal point, $pshed'_i$ is the shedding point, eps'_i is the distance between the pivotal point and the center of the Lamb discrete vortex and σ_0 is the Lamb vortex core).

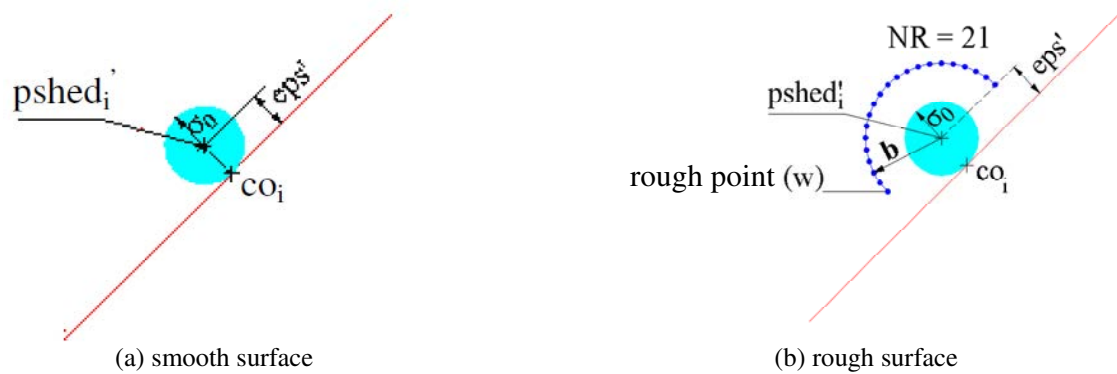


Figure 2. Vorticity generation process on the Discrete Vortex Method

The problem is solved by taking the curl of Eq. (3) and considering Eq. (2) to obtain the vorticity equation. For a 2-D flow this equation is scalar (the pressure term is absent), and it can be written as:

$$\frac{\partial \bar{\omega}}{\partial t} + (\bar{\mathbf{u}} \cdot \nabla) \bar{\omega} = \frac{I}{Re_c} \nabla^2 \bar{\omega} \quad (11)$$

where $Re_c = U^* d^* / \nu + \nu_i$ is the Reynolds number modified by eddy viscosity.

Depending on the Reynolds number flow, a roughness surface can stimulate the development of turbulence in the flow. The roughness model developed in this work is based on this physical sense. Thus, the second-order velocity structure function of the filtered field (Eq. (5)) is used with some adaptations in order to obtain the turbulent activity around the shedding point of each panel.

In order to determine the turbulent activity around the shedding point of an i panel ($pshed'_i$ point shown in Fig. 2(b)), a semicircle centered on shedding point i with radius $\|\mathbf{b}\| = 2\varepsilon - eps'_i$ is defined ($\varepsilon = \varepsilon^* / d^*$). A point set, called rough points, are defined on the semicircle. The average speed differences necessary to determine the second-order velocity structure function of the filtered field (see Eq. (5)) is computed between the center of the semicircle ($pshed'_i$ point) and the rough points. Thus:

$$\bar{F}_2(t) = \frac{I}{NR} \sum_{w=1}^{NR} \|\bar{\mathbf{u}}_i(\mathbf{x}_i, t) - \bar{\mathbf{u}}_w(\mathbf{x}_i + \mathbf{b}, t)\|_{w}^2 (I + \varepsilon) \quad (12)$$

where \mathbf{u}_i is the velocity on the points, NR is the number of rough points and $(I + \varepsilon)$ represents the kinetic energy gain due to the roughness effects. The authors used 21 rough points on each semicircle defined around each shedding point; this number is enough to obtain a reasonable value for the average speed differences.

The eddy viscosity associated to the shedding point of panel i , taking into account the roughness effects is given by (compare with Eq. (4)):

$$\nu_i(t) = 0.105 C_k^{-3/2} \sigma_{0_k} \sqrt{\bar{F}_2(t)} \quad (13)$$

where σ_{0_k} is the vortex core of the k discrete vortex positioned at i shedding point (see Fig. 2(b)).

As consequence, the Reynolds number needs to be modified:

$$Re_{c_i}(t) = \frac{U^* d^*}{\nu + \nu_i(t)} \quad (14)$$

It is important to say that the Reynolds number modification occurs locally, just on the discrete vortices shedding point, and when the roughness effects are important ($\nu_i(t) \neq 0$).

Equation (10) shows the relation between the Lamb vortex core and the Reynolds number. If the roughness effects are important ($\nu_i(t) \neq 0$), the Lamb vortex core must be modified. Thus:

$$\sigma_{oc_k}(t) = 4.48364 \sqrt{\frac{\Delta t}{Re} \left(1 + \frac{\nu_i(t)}{\nu} \right)} \chi \quad (15)$$

where σ_{oc_k} is the vortex core of the k discrete vortex positioned at i shedding point, modified by roughness model.

As consequence, depending on the roughness effects, the discrete vortex shedding position can be modified during all the time of the numerical simulation. Figure 3 shows the inertial effect imposed on the boundary layer flow due to the roughness surface model.

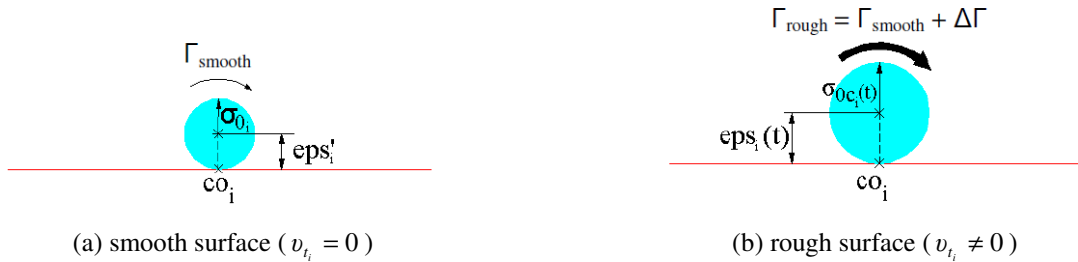


Figure 3. Inertial effect imposed by roughness surface model in the discrete vortices generation process

It is important to emphasize that there is no change on the body surface. The roughness surface effects are taken into account in the discrete vortices generation process. The roughness model developed here is based only on the physics of turbulent flows.

3.2 The Viscous Splitting Algorithm

The governing equation in 2-D Vortex Methods is the vorticity transport equation shown in Eq. (11). Chorin (1973) proposed an algorithm that splits convective-diffusive operator of Eq. (11) in the form:

$$\frac{D\bar{\omega}}{Dt} = \frac{\partial \bar{\omega}}{\partial t} + (\bar{\mathbf{u}} \cdot \nabla) \bar{\omega} = 0 \quad (16)$$

$$\frac{\partial \bar{\omega}}{\partial t} = \frac{1}{Re_c} \nabla^2 \bar{\omega} \quad (17)$$

According to the Lagrangian form of Eq. (16), the convective process is solved using a first order Euler scheme, after to compute the velocity vector field at each discrete vortex k present in the fluid domain. The velocity vector field is composed by three contributions: (i) the mainstream speed, $\bar{u}(\mathbf{x}, t)$, Eq. (18); (ii) the solid boundaries (Panel's Method, Katz and Plotkin, 1991), $\bar{u}^b(\mathbf{x}, t)$, Eq. (19); (iii) the vortex-vortex interaction (the Biot-Savart Law), $\bar{u}^v(\mathbf{x}, t)$, Eq. (20). Thus:

$$\bar{u}_1 = 1 \quad \text{and} \quad \bar{u}_2 = 0 \quad (18)$$

$$\bar{u}_k^n(\mathbf{x}_k, t) = \sum_{p=1}^{NP} \sigma_p c_{kp}^n [\mathbf{x}_k(t) - \mathbf{x}_p], \quad n = 1, 2 \quad \text{and} \quad k = 1, NV \quad (19)$$

Bimbato, A. M., Alcântara Pereira, L. A. and Hirata, M. H.
Numerical Investigation of the Drag Crisis in Flow Past a Rough Circular Cylinder

$$\overline{uv}_k^n(\mathbf{x}_k, t) = \sum_{j=1}^{NV} \Gamma_j c_{kj}^n [\mathbf{x}_k(t) - \mathbf{x}_j(t)], \quad n = 1, 2 \quad \text{and} \quad k = 1, NV \quad (20)$$

where NV is the total number of discrete vortices present in the flow at instant t , NP is the total number of source flat panels, $\sigma_p = \text{constant}$ is the source density per unit length, $c_{kp}^n[\mathbf{x}_k(t) - \mathbf{x}_p]$ is the n -th component of the velocity induced at discrete vortex k by p panel, Γ_j is the intensity of the j vortex and $c_{kj}^n[\mathbf{x}_k(t) - \mathbf{x}_j(t)]$ is the n -th component of the induced velocity at a discrete vortex k by a discrete vortex j . Note that the intensity Γ_j of each discrete vortices are determined using the no-slip condition and the source strengths are determined using the impermeability condition. These equations are satisfied simultaneously during each time step of the simulation.

In this paper, the viscous diffusion (Eq. (17)) is simulated using a fractional random walk method introduced by Chorin (1973):

$$\varsigma_k(t) = \sqrt{\frac{4 \Delta t}{Re_c} \ln\left(\frac{1}{P}\right)} [\cos(2\pi Q) + \sin(2\pi Q)] \quad (21)$$

where P and Q are random numbers, being $0 < P < 1$ and $0 < Q < 1$.

3.3 The Turbulence Model

Equation (21) shows that turbulence effects must be considered in diffusion process. Thus, in this stage there is a connection between the larger scales and the smaller ones, which is made by eddy viscosity (Eq. (4)). As described in Section 2, the local turbulent activities are determined by the second-order velocity structure function of the filtered field (Eq. (5)), which must be adapted to the two-dimensional problem, according to (Alcântara Pereira, *et al.*, 2002): (i) the points where velocities must be calculated are placed inside a circular crown centered at a reference vortex j , defined by $r_{int} = 0.1\sigma_{o_j}$ and $r_{ext} = 4.0\sigma_{o_j}$, where r_{int} and r_{ext} are the internal and external radius of the circular crown, respectively, and σ_{o_j} is the core of the Lamb discrete vortex under analysis. A statistical analysis was done by Bimbato, *et al.* (2012) to determine r_{int} and r_{ext} ; (ii) to compute the second-order velocity structure function of the filtered field, the points where velocities are calculated are the same as the positions of the vortices, which are near the vortex under analysis (inside the circular crown). Thus:

$$\overline{F}_{2_j} = \frac{1}{N} \sum_{k=1}^N \left\| \overline{\mathbf{u}}_{r_j}(\mathbf{x}_j) - \overline{\mathbf{u}}_{r_k}(\mathbf{x}_j + \mathbf{r}_k) \right\|_k^2 \left(\frac{\sigma_{o_j}}{\mathbf{r}_k} \right)^{2/3} \quad (22)$$

where $\overline{\mathbf{u}}_i$ is the total velocity in the point ($\overline{\mathbf{u}}_i = \overline{ui} + \overline{ub} + \overline{uv}$), N indicates the number of discrete vortices inside the circular crown and \mathbf{r}_k is the distance between the discrete vortex under analysis (j -th discrete vortex) and the discrete vortices inside the circular crown (each k -th discrete vortex).

3.4 Aerodynamic Loads

With the vorticity field it is possible to obtain a Poisson equation for the pressure and its solution is obtained through the following integral formulation (Shintani and Akamatsu, 1994):

$$H\overline{Y}_p - \int_{S_i} \overline{Y}\nabla\varepsilon_p \cdot \mathbf{e}_n dS = \iint_{\Omega} \nabla\varepsilon_p \cdot (\overline{\mathbf{u}} \times \overline{\boldsymbol{\omega}}) d\Omega - \frac{1}{Re} \int_{S_i} (\nabla\varepsilon_p \times \overline{\boldsymbol{\omega}}) \cdot \mathbf{e}_n dS \quad (23)$$

where the pressure is computed at p -th pivotal point, co (see Fig. 2), $H = 1.0$ in the fluid domain, $H = 0.5$ on the boundaries, ε is a fundamental solution of Laplace Equation, \overline{Y} is the specific work and \mathbf{e}_n is the unit vector normal to each source flat panel. The drag and lift forces are obtained by pressure integration.

4. SIMULATIONS OF UNSTEADY FLOWS PAST A CIRCULAR CYLINDER

4.1 Smooth Circular Cylinder

There are many studies about the flow around a smooth cylinder available in the literature. This fact justifies the study of this problem as a first validation of some important numerical parameters, such as: the number of source flat panels used to represent the cylinder surface ($NP = 300$), the time increment ($\Delta t = 0.05$), and the Lamb vortex core ($\sigma_0 = 0.001$). The Reynolds number chosen is $Re = 1.0 \times 10^5$, which is a typical subcritical flow regime.

The strategy is to study the characteristics of the flow around a smooth cylinder. Then, in the next section, the roughness model will be applied. The main target is to obtain, with the roughness code, a supercritical flow regime from a typical subcritical flow regime of $Re = 1.0 \times 10^5$.

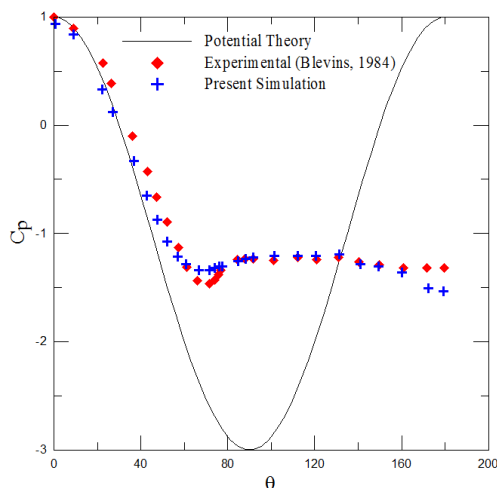
Table 1 show some experimental results from Blevins (1984) and the results obtained using our vortex code. The results of Blevins present 10% of uncertainty.

Table 1. Mean drag and lift coefficients and Strouhal number for the smooth circular cylinder.

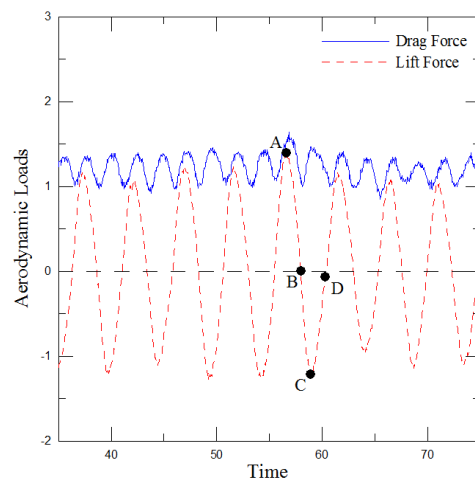
$Re = 1.0 \times 10^5$	\bar{C}_D	\bar{C}_L	St
Blevins (1984) - experimental	1.20	-	0.19
Present Simulation	1.223	0.021	0.207

The aerodynamic loads computations are evaluated between $37.50 \leq t \leq 75.00$ and as can be seen agree quite well with the experimental results. The present drag coefficient shows a higher value as compared to the experimental result. One should observe that the three-dimensional effects are non-negligible for the Reynolds number used in the present simulation ($Re = 1.0 \times 10^5$). Therefore, one can expect that a two-dimensional computation of such a flow must produce higher values for the drag coefficient. The mean numerical lift coefficient, although very small, is not zero which is due to numerical approximations.

Figure 4(a) shows the mean pressure distribution calculated for the smooth cylinder to be compared with the potential flow pressure distribution and the experimental values presented by Blevins (1984). The present result agrees well with the experimental ones. From Fig. 4(a), it can be observed that the predicted separation point occurs around $\theta \cong 77^\circ$, while the experimental value (Blevins, 1984) is around 82° . Hence, separation takes place in the laminar mode as expected for a subcritical Reynolds number flow.



(a) averaged pressure coefficient



(b) temporal series of drag and lift coefficients

Figure 4. Aerodynamic loads acting on a smooth circular cylinder ($Re = 1.0 \times 10^5$)

Figure 4(b) presents the time evolution of the aerodynamic forces. The drag force oscillates at a frequency that is twice the lift force frequency, which is a typical behaviour of an isolated and smooth circular cylinder; in fact the drag force oscillates every time that a vortex structure is shed from the upper or lower side of the cylinder. On the other hand, the lift force oscillates once for each pair of vortex structure shed. Figure 4(b) shows four important instants (points A, B, C and D) to explain the physics involved in this kind of flow.

At instant represented by point A, there is a low pressure distribution at upper cylinder surface (between $\theta \cong 59^\circ$ and $\theta \cong 180^\circ$), which explains the maximum lift force (Fig. 4(b)). The lower pressure distribution region corresponds to a clockwise vortex structure that was shed on the upper side of the cylinder (see Fig. 5(d)) and now, at instant A, is on its initial development stage (see Fig. 6 (point A) and Fig. 5(a)). This initial development stage is the responsible for drag force increase (see drag curve in Fig. 4(b), at instant A).

Bimbato, A. M., Alcântara Pereira, L. A. and Hirata, M. H.
Numerical Investigation of the Drag Crisis in Flow Past a Rough Circular Cylinder

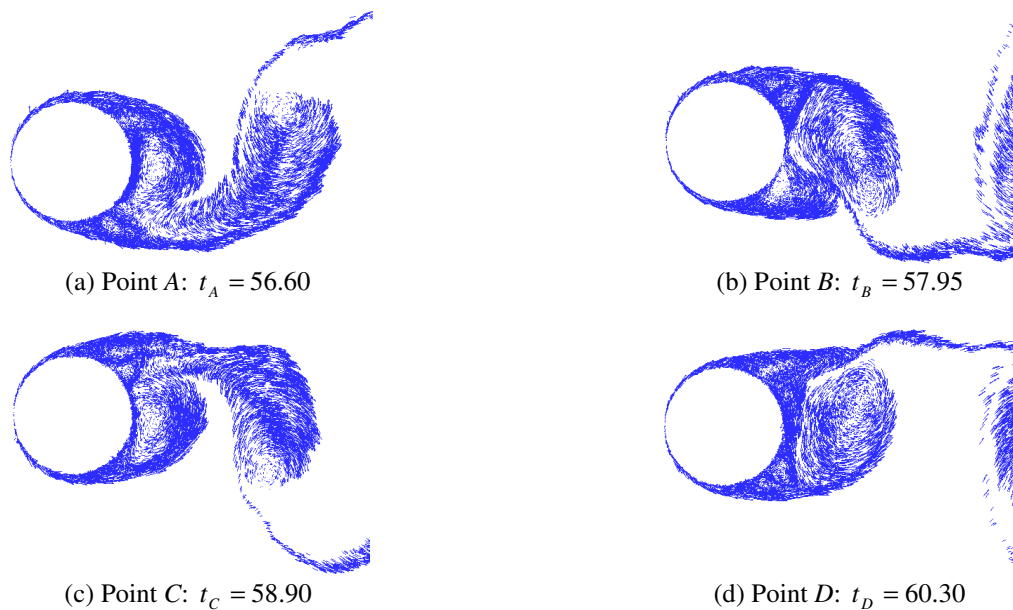


Figure 5. Near wake behaviour for smooth circular cylinder ($Re = 1.0 \times 10^5$)

At instant B , the upper clockwise vortex structure continues growing. Now it is attracting the opposite shear layer (see Fig. 5(b)). At the same time, a counter-clockwise vortex structure is shed on the lower side of the cylinder.

At instant represented by point C , there is a low pressure distribution at lower cylinder surface (between $\theta \cong 180^\circ$ and $\theta \cong 296^\circ$), which explains the minimum lift force (Fig. 4(b)). The lower pressure distribution region corresponds to a counter-clockwise vortex structure that was shed on the lower side of the cylinder at instant B . Now, at instant C , this counter-clockwise vortex structure is on its initial development stage (see Fig. 6 (point C) and Fig. 5 (c)). This initial development stage is the responsible for drag force increase (see drag curve in Fig. 4(b), at instant C). Simultaneously, the counter-clockwise vortex structure starts to grow attracting the opposite shear layer which is feeding the clockwise vortex structure causing its detachment (Fig. 5(c)).

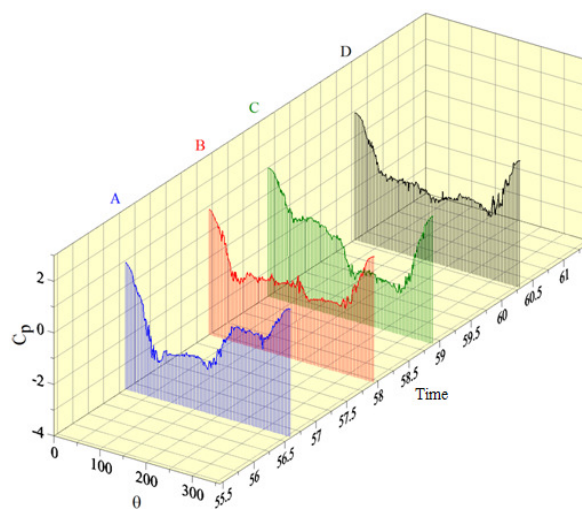


Figure 6. Instantaneous pressure distribution on the surface of a smooth circular cylinder ($Re = 1.0 \times 10^5$)

At instant D , the upper clockwise vortex structure is definitely incorporated by the viscous wake (Fig. 5(d)). Likewise, a new clockwise vortex structure is born in the upper cylinder surface and begins to grow attracting the lower shear layer which is feeding the counter-clockwise vortex structure causing its detachment (Fig. 5(a)). At instant B , the lower counter-clockwise vortex structure is definitely incorporated by the viscous wake (Fig. 5(b)).

It can be seen that the mechanism of vortex shedding described above is in agreement to the one proposed by Gerrard (1966); it is repeated periodically causing the oscillating von kármán street as shown in Fig. 7.

Since the flow around a smooth circular cylinder is well predicted, we are able to use the same numerical parameters used in this section to implement our roughness model.

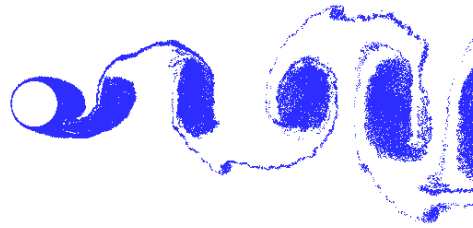


Figure 7. Final position of the vortices for the flow past a smooth circular cylinder ($Re = 1.0 \times 10^5$)

4.2 Rough Circular Cylinder

The aim of this section is to prove that the roughness model can develop turbulent boundary layer flows from subcritical Reynolds number flow of $Re = 1.0 \times 10^5$.

Table 2 shows comparisons between the aerodynamic behaviour of the smooth cylinder and the rough cylinder; θ_{sep} is the angle where the boundary layer separation takes place (it is defined according to Fig. 1).

Table 2. Influence of the roughness model in the flow around a circular cylinder ($Re = 1.0 \times 10^5$).

ϵ	$\overline{C_D}$	$\overline{C_L}$	St	θ_{sep}
0.000	1.223	0.021	0.207	77°
0.001	1.188	0.035	0.206	81°
0.002	1.133	0.005	0.203	81°
0.007	1.071	-0.132	0.191	88°

It can be seen from Tab. 2 that the smaller roughness tested ($\epsilon = 0.001$ and $\epsilon = 0.002$) cause just a small perturbation in the boundary layer flow. The flow separation occurs at $\theta \cong 81^\circ$ which is almost that one verified for the smooth cylinder. However it can be noted (see Tab. 2) the beginning of the drag crisis. As the drag crisis is just starting no modification on vortex shedding frequency occurs ($St \cong 0.2$). As consequence, one can say that this is a subcritical Reynolds number flow yet (see Fig. 8).

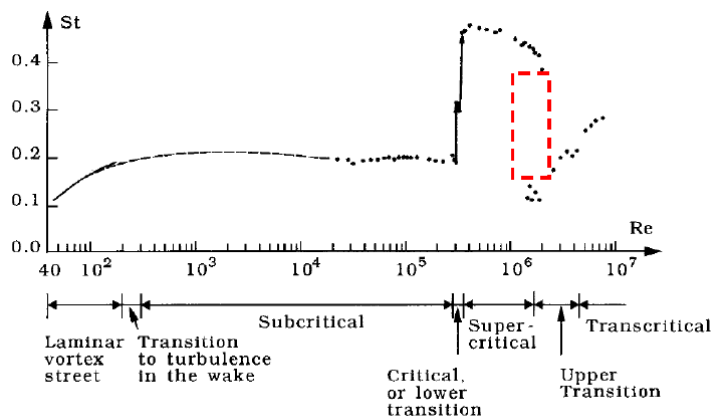


Figure 8. $St \times Re$ diagram of the flow around a smooth circular cylinder (Sumer and Fredsøe, 2006)

On the other hand, when the roughness model simulates a surface with relative roughness of $\epsilon = 0.007$ the flow regime is not subcritical anymore. Figure 9(a) shows the mean pressure distribution that acts on the rougher cylinder surface ($\epsilon = 0.007$).

In this situation, the boundary layer flow separates at $\theta \cong 88^\circ$, what means that the separation points move downstream (compare with the smooth cylinder in Tab. 2). As consequence, the drag coefficient is reduced about 12.4%. Computed values for drag and lift coefficients are plotted in Fig. 9(b). The amplitude of periodical oscillations seen in Fig. 4(b) are now smaller but with much noise. When $\epsilon = 0.007$ the Strouhal number is reduced from approximately 0.21 ($\epsilon = 0.000$) to approximately 0.19.

Figure 9(b) shows four important instants (points A, B, C and D) which help to explain the vortex shedding frequency decrease and the change on the flow regime. The pressure distribution at each instant highlighted in Fig. 9(b)

Bimbato, A. M., Alcântara Pereira, L. A. and Hirata, M. H.
Numerical Investigation of the Drag Crisis in Flow Past a Rough Circular Cylinder

is shown in Fig. 10. It can be seen that the vortex shedding mechanism is modified by roughness effects. One can see in Fig. 10 that roughness causes oscillations at instantaneous pressure distributions (compare with Fig. 6).

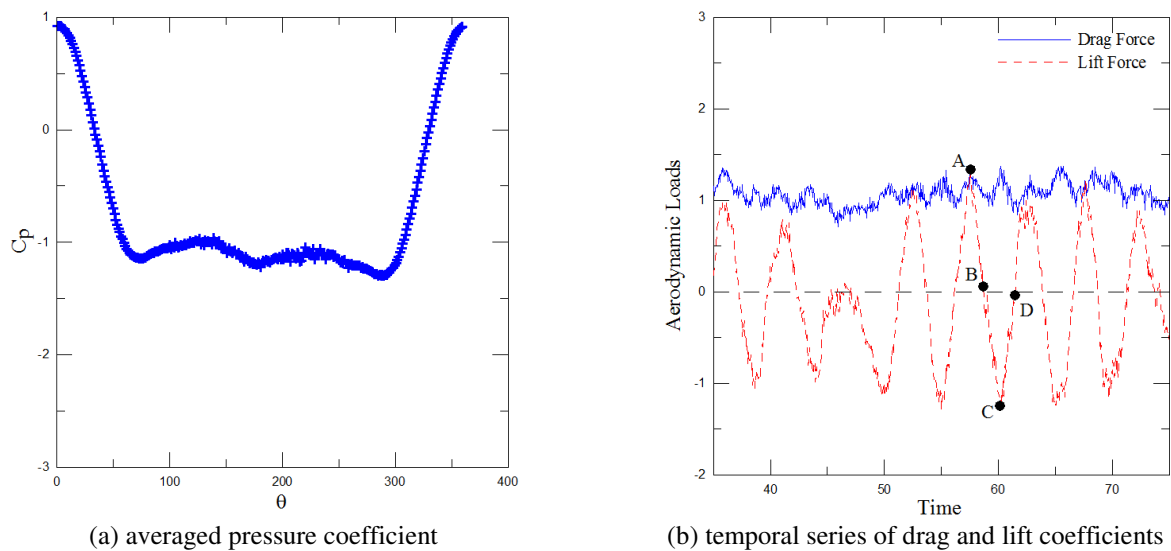


Figure 9. Aerodynamic loads acting on a rough circular cylinder ($Re = 1.0 \times 10^5$; $\varepsilon = 0.007$)

The changes in flow behaviour were expected since the roughness tested ($\varepsilon = 0.007$) is able to cause supercritical flows (Fage and Warsap, 1929; Zdravkovich, 2003). So, based on the delay in the boundary layer separation (from $\theta \cong 77^\circ$ to $\theta \cong 88^\circ$) and on the drag coefficient decrease (from $\overline{C}_D = 1.223$ to $\overline{C}_D = 1.071$), we can say that our roughness model simulated the turbulent flow characteristics.

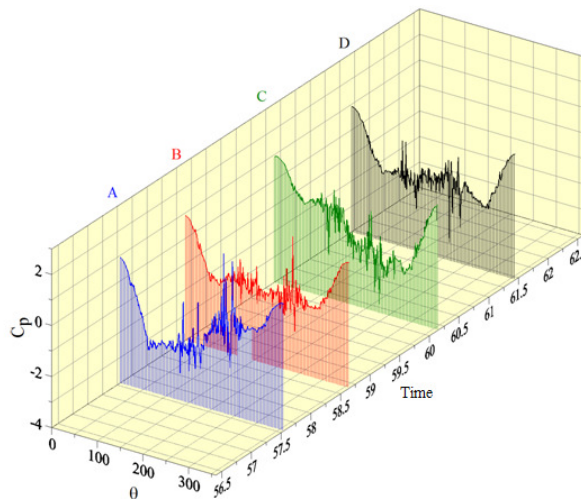


Figure 10. Instantaneous pressure distribution on the surface of a rough circular cylinder ($Re = 1.0 \times 10^5$; $\varepsilon = 0.007$)

However it is necessary to explain an important question: if the boundary layer separation was delayed why the Strouhal number decreased; one should expect an increase on vortex shedding frequency.

The most important feature of supercritical flow is the vortex shedding suppression (please, see the highlighted region in Fig. 8). However, as the Reynolds number increases, the vortex shedding appears again, but at an irregular manner (at the end of supercritical flow regime and in the upper transition flow regime). When the flow reaches the transcritical flow regime the vortex shedding occurs at a regular manner again.

Thus, the vortex shedding frequency decrease occurs because the flow reached a transition regime, between the supercritical regime (where the vortex shedding is suppressed) and the transcritical regime (where the vortex shedding occurs normally).

Figure 11 shows the velocity field at instants *A*, *B*, *C* and *D*.

It can be seen the same vortex shedding mechanism described for the smooth cylinder. However, when $\varepsilon = 0.007$ the mechanism is delayed which explains the Strouhal number decrease.

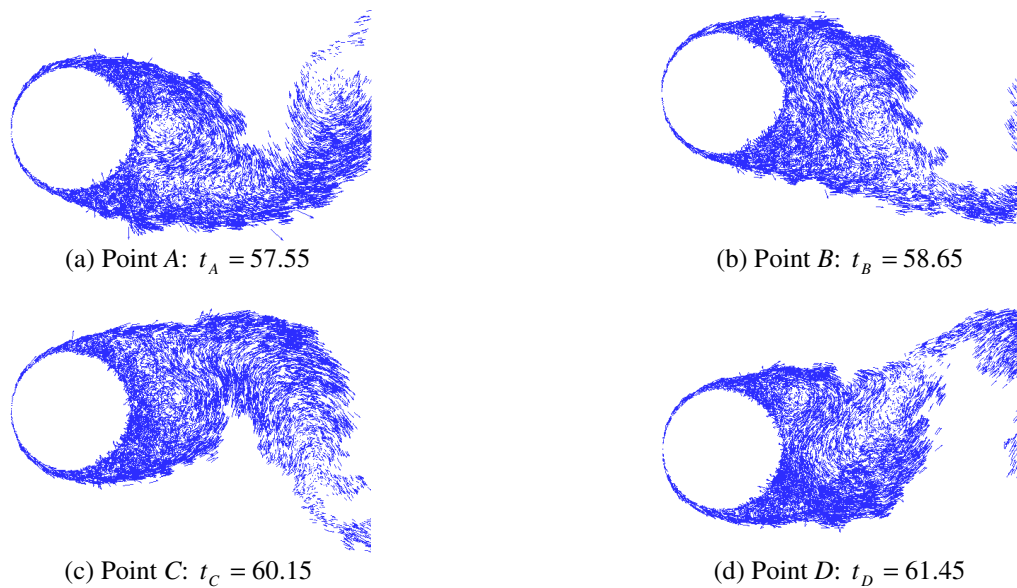


Figure 11. Near wake behaviour for rough circular cylinder ($Re = 1.0 \times 10^5$; $\varepsilon = 0.007$)

The upper clockwise vortex structure is shed and remains at the rear part of the cylinder for a longer time; the same occurs with the lower counter-clockwise vortex structure. As described in Section 4.1, the development of each vortex structure (upper clockwise one or lower counter-clockwise one) is the responsible to cause the detachment of the other one (lower counter-clockwise one or upper clockwise one). Since the vortices structures development is delayed, the vortex shedding will be delayed as well. In other words, the Strouhal number is decreased.

This delayed process occurs periodically for the rougher cylinder, causing the oscillating wake shown in Fig. 12.

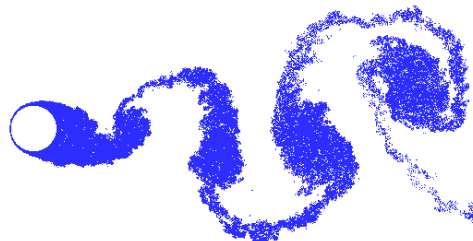


Figure 12. von Kármán street developed downstream a rough circular cylinder ($Re = 1.0 \times 10^5$; $\varepsilon = 0.007$)

Compare Fig. 12 with Fig. 7 and see how the roughness model makes the von Kármán street narrower. This is a consequence of the delay in the boundary layer separation point which causes the drag crisis.

5. CONCLUSIONS

The roughness model developed in this paper imposes an inertial effect on the nascent discrete vortices in order to simulate what happens in a turbulent boundary layer flow. There is no change on solid boundary characteristics. The model is based on the physical sense that roughness surfaces can promote transition to turbulence in boundary layers.

It is known that a single two-dimensional turbulence model may not make sense, since the turbulence is essentially three-dimensional. However, the results showed that the turbulence model associated with a roughness model can represent important flow features, even in a 2-D simulation. The example is the drag crisis captured by our new code.

The comparisons between the numerical results and experimental ones were avoided due to the difficulty to determine exactly the roughness surface characteristics, especially the surface texture. According to the experimental studies made by Guven, *et al.* (1980) this parameter can cause differences on the measured drag coefficient about 60%.

Finally, the authors hope to develop a 3-D Vortex Method in a near future. In this context the roughness model developed in this paper seems to be very promising.

6. ACKNOWLEDGEMENTS

This study was supported by Brazilian Research Agency (CNPq), Proc. 142804/2008-8 and FAPEMIG.

Bimbato, A. M., Alcântara Pereira, L. A. and Hirata, M. H.
 Numerical Investigation of the Drag Crisis in Flow Past a Rough Circular Cylinder

7. REFERENCES

- Achenbach, E., 1971. "Influence of Surface Roughness on the Cross-Flow around a Circular Cylinder". *Journal of Fluid Mechanics*, Vol. 46, pp. 321-335.
- Alcântara Pereira, L. A., Ricci, J. E. R., Hirata, M. H. and Silveira Neto, A., 2002. "Simulation of the Vortex-Shedding Flow about a Circular Cylinder with Turbulence Modeling". *CFD Journal*, Vol. 11, n. 3, pp. 315-322, October.
- Batchelor, G. K., 1953. *The Theory of Homogeneous Turbulence*. Cambridge Univ. Press, Cambridge, England, UK.
- Bimbato, A. M., 2012. *Study of Turbulent Flows around a Smooth or a Rough Bluff Body Using the Discrete Vortex Method*, D.Sc. Thesis, Institute of Mechanical Engineering, UNIFEI, Itajubá, MG, Brazil (in Portuguese).
- Bimbato, A. M., Alcântara Pereira, L. A. and Hirata, M. H., 2012. "Corrected Lagrangian LES Model for Vortex Method". *8th Spring School on Transition and Turbulence*, São Paulo, Sep. 24-28.
- Blevins, R. D., 1984. *Applied Fluid Dynamics Handbook*. Van Nostrand Reinhold Co.
- Buresti, G., 1981. "The Effect of Surface Roughness on the Flow Regime around Circular Cylinders". *Journal of Wind Engineering & Industrial Aerodynamics*, Vol. 8, pp. 115-122.
- Chorin, A. J., 1973. "Numerical Study of Slightly Viscous Flow". *Journal of Fluid Mechanics*, Vol. 57, pp. 785-796.
- Fage, A. and Warsap, J. H., 1929. "The Effects of Turbulence and Surface Roughness on the Drag of a Circular Cylinder". *Brit. Aeronautical Research Council*, Rep and Memo 1283.
- Gerrard, J. H., 1966. "The Mechanics of the Formation Region of Vortices behind Bluff Bodies". *J. Fluid Mech.* 25:401-13.
- Güven, O., Farell, C. and Patel, V. C., 1980. "Surface Roughness Effects on the Mean Flow Past Circular Cylinders". *Journal of Fluid Mechanics*, Vol. 98, pp. 673-701.
- Kamemoto, K., 2004. "On Contribution of Advanced Vortex Element Methods toward Virtual Reality of Unsteady Vortical Flows in the New Generation of CFD". *J. Braz. Soc. Mech. Sci. & Eng.*, Vol. 26, n. 4, Rio de Janeiro, Oct. / Dec..
- Kareem, A. and Cheng, C. M., 1999. "Pressure and Force Fluctuations on Isolated Roughened Circular Cylinders of Finite Height in Boundary Layer Flows". *Journal of Fluids and Structures*, Vol. 13, pp. 907-933.
- Katz, J. and Plotkin, A., 1991. *Low Speed Aerodynamics: From Wing Theory to Panel Methods*. McGraw Hill, Inc.
- Kawamura, T., Takami, H. and Kuwahara, K., 1986. "Computation of High Reynolds Number Flow around a Circular Cylinder with Surface Roughness". *Fluid Dynamics Research*, Vol. 1, pp. 145-162.
- Kundu, P. K., 1990. *Fluid Mechanics*, Academic Press.
- Leonard, A., 1980. "Vortex Methods for Flow Simulation". *Journal of Computational Physics*, Vol. 37, pp. 289-335.
- Lesieur, M. and Métais, O., 1996. "New Trends in Large Eddy Simulation of Turbulence". *A Review in Fluid Mechanics*, Vol. 28, pp. 45-82.
- Lewis, R. I., 1999. "Vortex Element Methods, The Most Natural Approach to Flow Simulation - A Review of Methodology with Applications". *Proc. of 1st Int. Conf. on Vortex Methods*, Kobe, Nov. 4-5, pp. 1-15.
- Mustto, A. A., Hirata, M. H. and Bodstein, G. C. R., 1998. "Discrete Vortex Method Simulation of the Flow around a Circular Cylinder with and without Rotation". A.I.A.A. Paper 98-2409, *Proceedings of the 16th A.I.A.A. Applied Aerodynamics Conference*, Albuquerque, NM, USA, June.
- Nishino, T., 2007. *Dynamics and Stability of Flow past a Circular Cylinder in Ground Effect*. Ph.D. Thesis, Faculty of Engineering Science and Mathematics, University of Southampton.
- Roshko, A., 1961. "Experiments on the Flow past a Circular Cylinder at Very High Reynolds Number". *Journal of Fluid Mechanics*, Vol. 10, pp. 345-356.
- Shintani, M., Akamatsu, T., 1994. Investigation of Two-Dimensional Discrete Vortex Method with Viscous Diffusion Model. *CFD Journal*, vol. 3, n. 2, pp. 237-254.
- Smagorinsky, J., 1963. "General Circulation Experiments with the Primitive Equations". *Mon. Weather Rev.*, Vol. 91, n. 3, pp. 99-164.
- Stock, M. J., 2007. *Summary of Vortex Methods Literature (A lifting document rife with opinion)*. April, 18: © 2002-2007 Mark J. Stock.
- Sumer, B. M. and Fredsøe, J., 2006. "Hydrodynamics around Cylindrical Structures". *Advanced Series on Ocean Engineering*, Vol. 26, 550p.
- Szechenyi, E., 1975. "Supercritical Reynolds Number Simulation for Two Dimensional Flow over Circular Cylinders". *Journal of Fluid Mechanics*, Vol. 70, pp. 529-542.
- Zdravkovich, M. M., 2003. *Flow around Circular Cylinders. Vol. 2: Applications*. Oxford University Press, Oxford, U.K.

8. RESPONSIBILITY NOTICE

The authors are the only responsible for the printed material included in this paper.